Title: The glucocorticoid-induced leucine zipper (gilz/Tsc22d3-2) gene locus plays a crucial role in male fertility.
Authors: Suarez PE, Rodriguez EG, Soundararajan R, Mérillat AM, Stehle JC, Rotman S, Roger T, Voirol MJ, Wang J, Gross O, Pétrilli V, Nadra K, Wilson A, Beermann F, Pralong FP, Maillard M, Pearce D, Chrast R, Rossier BC, Hummler E
Journal: Molecular endocrinology (Baltimore, Md.)
Year: 2012 Jun
Volume: 26
Issue: 6
Pages: 1000-13
DOI: 10.1210/me.2011-1249

The glucocorticoid-induced leucine zipper (Gilz/*Tsc22d3-2*) gene locus plays a crucial role in male fertility

Philippe E. Suarez[1,11*], Elena Gonzalez Rodriguez[1*], Rama Soundararajan[2], Anne-Marie Mérillat[1], Jean-Christophe Stehle[3], Samuel Rotman[3], Thierry Roger[4], Marie-Jeanne Voirol[5], Jian Wang[2], Olaf Gross[6], Virginie Pétrilli[6,12], Karim Nadra[7], Anne Wilson[8], Friedrich Beermann[9], François P. Pralong[5], Marc Maillard[10], David Pearce[2], Roman Chrast[7], Bernard C. Rossier[1], Edith Hummler[1]

Affiliations:

[1] Department of Pharmacology and Toxicology, University of Lausanne, Switzerland

[2] Division of Nephrology, Department of Medicine, University of California, San Francisco, USA

[3] Institute of Pathology, CHUV, Lausanne, Switzerland

[4] Service of Infectious Diseases, Department of Medicine, CHUV and University of Lausanne, Lausanne, Switzerland

[5] Service of Endocrinology, Diabetology and Metabolism, Department of Medicine, CHUV and University of Lausanne, Switzerland

[6] Department of Biochemistry, University of Lausanne, Epalinges, Switzerland

[7] Department of Medical Genetics, University of Lausanne, Switzerland

[8] Ludwig Centre for Cancer Research of the University of Lausanne (LICR@UNIL), 1066 Epalinges, Switzerland

[9] ISREC SV EPFL, Lausanne, Switzerland

[10] Service of Nephrology, CHUV, Lausanne, Switzerland.

* Authors contributed equally.

Present address:

[11] Division of Molecular Pediatrics, Centre Hospatalier Universitaire Vaudois, Clinique Infantil, Lausanne, Switzerland

[12]Université de Lyon; Inserm U1052; CNRS UMR5286, Centre de Recherche en Cancérologie de Lyon; 69000 Lyon, France

Reprint request to :

Dr. Edith Hummler (corresponding author)

Department of Pharmacology and Toxicology, Rue du Bugnon 27, CH-1005 Lausanne, Switzerland; Fax: +41 21 6925355; Phone: +41 21 6925357; e-mail: Edith.Hummler@unil.ch

Running Title: **Male sterility in Gilz-deficient mice**

Key words: Glucocorticoids, metabolism, sterility, sodium homeostasis, ENaC, inflammation

Grants supporting this study:

Fondation Emma Muschamps, Swiss National Science Foundation, Leducq Foundation to EH; Swiss National Science Foundation, Association "Institute for Arthritis Research" and Louis-Jeantet Prize for Medicine to Jürg Tschopp and his collaborators OG and VP; Marie Curie fellowship to VP;

No disclosure

Abstract

The glucocorticoid-induced leucine zipper (Gilz, *Tsc22d3-2*) is a widely expressed dexamethasone-induced transcript that has been proposed to be important in immunity, adipogenesis and renal sodium handling based on in vitro studies. To study its function in vivo, we have used Cre/lox technology to generate mice deficient for *Tsc22d3-2*. Male knockout were viable, but surprisingly did not show any major deficiencies in immunological processes or inflammatory responses. *Tsc22d3-2* knockout mice adapted to a sodium-deprived diet and to water deprivation conditions, but developed a subtle deficiency in renal sodium and water handling. Moreover, the affected animals developed a mild metabolic phenotype revealed by a reduction in weight from 6 months of age, mild hyperinsulinemia and resistance to a high fat diet. *Tsc22d3-2*-deficient males were infertile and exhibited severe testis dysplasia from postnatal day 10 onwards with increases in apoptotic cells within seminiferous tubules, an increased number of Leydig cells, and significantly elevated FSH and testosterone levels. Thus our analysis of the *Tsc22d3-2*-deficient mice demonstrated a previously uncharacterized function of GILZ protein in testis development.

Introduction

Glucocorticoids are involved in the physiological regulation of a variety of processes including immune responses, metabolism, cell growth and development. Due to their anti-inflammatory and immunosuppressive roles, they are widely used in the clinic to treat inflammation, allergy or malignancies (reviewed in Ayroldi and Riccardi, 2009 (1)). The X-linked glucocorticoid-induced leucine zipper (GILZ, *Tsc22d3-2*) was originally identified as a dexamethasone-induced transcript protecting T lymphocytes from TCR/CD3-activated cell death (2). TSC22D3-2 encodes a new member of the TSC22-domain leucine zipper family and is expressed in a variety of different organs and tissues. Members of this family (TSC22D1 to TSC22D4) share a highly conserved TSC- (tuberous sclerosis complex)- and a PDZ (post synaptic density protein; PSD95) box domain (reviewed in Ayroldi and Riccardi, 2009 (1)). TSC22D3-2 homo- or heterodimerizes by means of its leucine zipper domain (3). In total, four isoforms have been characterized as splice variants of the TSC22D3-2 gene, and named GILZ1-4 (4). Although these four isoforms are present with varying

abundance in mouse and rat tissues, they are not functionally redundant but rather involved in distinct aspects of cellular physiology and may therefore modulate different signaling pathways (4). Moreover, due to multiple protein interactions in a variety of cell types, TSC22D3-2 has not only been implicated in apoptosis and cell proliferation, but also in the modulation of T lymphocyte activation and IL2-production (5-7), and in dendritic cell function (8, 9). Furthermore, TSC22D3-2 was shown to inhibit Ras-induced cell proliferation (6) and to mediate renal sodium transport (10, 11) or adipogenesis (12).

In the present report, we have generated a mouse model constitutively lacking all main isoforms of TSC22D3-2 (4). Male mice lacking TSC22D3-2 are viable, and show no abnormalities in the immune system, in adipogenesis or sodium reabsorption. However, mating and histological analyses revealed that loss of TSC22D3-2 leads to male sterility.

Results

Generation of *Tsc22d3-2* knockout mice

We generated mice with a *Tsc22d3-2* knockout allele (**Fig. S1**). When heterozygous mutant females were bred to wildtype males, deficient male mice (*Tsc22d3-2*$^{\Delta/y}$) were born according to the expected Mendelian distribution (male y/+ crossed with female Δ/+; from a total of 181 offspring analysed: males, 47 (+/+) and 52 (Δ/+); females, 41 (+/+) and 41 (Δ/+; 7.7 ±2.5 pups per litter, N= 20 litters). The heterozygous mutant females were mated at the age of about 10 weeks, kept up to 6 months and up to six consecutive litters were registered. In contrary, when 3 mating cages were set with one knockout male (3-6 months old) and two C57BL/6N females (8-12 weeks, replaced every three weeks), we could never observe pregnancies and/or born litters. This strongly suggested a male sterility problem. In wild type mice, levels of *Tsc22d3-2* were highest in kidney, brain, lung and heart, with moderate expression in thymus, liver and skin and relatively low levels in testis and spleen (**Fig. S2*A***). In mice, *Tsc22d3-2* mRNA and protein expression was lacking (**Fig. S2*B***). The GILZ1 isoform is normally present in thymus, spleen and lung, whereas GILZ2 is detected in testis liver, skin and brain; both of these isoforms were missing in the knockout **(Fig. S2*C*)**. This

demonstrates that the *Tsc22d3-2* gene locus was efficiently deleted in *Tsc22d3-2*$^{\Delta/y}$ mice resulting in the absence of the major GILZ isoforms.

Tsc22d3-2$^{\Delta/y}$ mice show mild metabolic alterations with age

Knockout mice were born with normal body weight and gained weight normally until about 6 months of age, but then slowed significantly (**Fig. 1*A***; **Table S1**; $P< 0.05$). Body length and body fluids were unaltered, but fat values were significantly reduced in old knockout mice (**Table S1**; $P < 0.05$). Plasma insulin and glucose levels measured in knockout and control mice kept under fed, fasted and refed states revealed a significantly higher plasma insulin level upon normal feeding (**Table S2**; $P < 0.05$), while plasma glucose levels were unchanged. Upon fasted and refed conditions, both groups exhibited no significant changes in plasma insulin levels (**Table S2**), or impairment in the glucose and insulin tolerance test, although recovery of plasma glucose concentration was slowed (**Fig. 1*B* and *C***). Interestingly, pancreas sections stained for insulin and glucagon levels revealed significantly more glucagon secreting a-cells in the knockout group per islet despite unchanged plasma glucagon levels (**Fig. 1*D* and *E*;** $P < 0.01$). After 18 weeks on a high-fat diet knockout mice showed significantly less weight and body fat content (Echo MRI analysis) (**Fig. 1*G* and Table 1**). Insulin levels were similar in all groups, with the exception of higher insulin levels in the knockout group fed with a normal diet (**Table 2; Fig. 1*G***). Interestingly, following a high fat diet liver histology revealed that the knockout mice appear protected from developing hepatic steatosis (**Fig. 1*H***).

We next exposed mouse embryonic fibroblasts (MEFs) to an adipogenic cocktail. Following Oil-Red O-staining, the percentage of MEFs differentiating into adipocytes was similar in the knockout and control (**Fig. 1*I* and *J***). In parallel, quantitative RT-PCR measurements revealed no difference in basal *Pparγ2* mRNA expression in nondifferentiated MEFs, while the basal fatty acid binding protein 4 (*FABP4, aP2*) mRNA transcript expression level was already significantly increased in the knockout mice (**Fig. 1*K***). Upon differentiation into adipocytes, *Pparγ2* and *Fabp4* mRNA transcript expression levels were increased in both groups, and significantly elevated in the knockout group (**Fig. 1*K***). In the controls, *Tsc22d3-2* (Gilz) the mRNA transcript expression level was increased 4-fold upon differentiation (**Fig. 1*K***). Quantitative RT-PCR analyses on adipose tissue from control and

knockout mice revealed no differences in the expression of *Pparγ , Pparγ2 , Tsc22d1*, adiponectin, *FabP4* and Krüppel-like factor 15 (KlF15) (**Fig. 1*L***). In summary, *Tsc22d3-2*-deficient mice exhibited a relatively mild metabolic phenotype despite the observed higher insulin level. Our data demonstrated that in vitro adipogenesis was not affected by the absence of TSC22D3-2. However, mature adipocytes were unable to accumulate lipids normally, an effect which was further accentuated upon a high fat diet.

Tsc22d3-2 is not required for the development of the immune system, inflammatory response or sepsis

To test the role of *Tsc22d3-2* in the immune system, we first measured thymus weight at P10, P20 and following puberty. Although thymi were significantly smaller in the oldest knockout group, younger animals had normal absolute cell numbers (**Fig. 2*A*** and ***B*; *P*<** 0.05). FACS analysis of thymocyte subsets revealed no major changes in the mature single positive (SP) CD4 or CD8 populations. However, a reduced number of DN (double negative, CD4-CD8-) 3, (CD25+CD44-) immature thymocytes and a corresponding increase in DN4 (CD25-CD44-) thymocytes was observed (**Fig. 2*B***; *P*< 0.05). The glucocorticoid-sensitive thymocyte DP (double positive, $CD4^+$ $CD8^+$) subset of T cells is unaffected in *Tsc22d3-2*-knockout mice (**Fig. 2*B***). Similarly, with the exception of an increased number of erythroblasts, the absolute cell number of spleen subsets and lymph node subsets is not altered in the knockout groups (**Fig. 2*C*** and ***D***; *P*< 0.05). Overall, the architecture and cell distribution in the thymus and spleen from knockout mice was preserved (**Fig. S3**).

To further test whether the inflammatory immune response is altered in mice lacking TSC22D3-2, we measured TNF and MIP-2 cytokine secretion from bone marrow-derived macrophages upon stimulation with various inflammatory stimuli ± pretreatment with dexamethasone (**Fig. 3*A-C***). Under all conditions tested, we observed normal cytokine production in TSC22D3-2-deficient cells (**Fig. 3*A-C***). When bone marrow-derived dendritic cells (BMDCs) were treated with various stimuli (LPS, MSU, ATP, Candida and CpG), we found no differences in the secretion of IL-1b, TNF or RANTES (**Fig. 3*E-G***). Dexamethasone treatment or pretreatment with heat-inactivated candida cells led to a dose-dependent reduction in cytokine production that was unaffected by the loss of

TSC22D3-2 (**Fig. 3*E-G***). Furthermore, we tested whether *Tsc22d3-2* is implicated in a sepsis model and analysed cytokine secretion of IL-6, IL-12, TNF- and IL-2 in bone marrow-derived macrophages (BMDMs) upon various stimuli (**Fig. 4)**. No significant differences were observed, and BDMCs responded to dexamethasone administration in a dose-dependent manner (**Fig. 4*A-C***). Splenocytes when stimulated by anti-CD3 plus anti-CD28 or concanavalin A, exhibited a dose-dependent response independent of TSC22D3-2 (**Fig. 4*D, E***). Altogether, our experiments suggest that TSC22D3-2 is not of major importance in immunological processes or inflammatory responses.

TSC22D3-2-deficient mice present slightly impaired renal sodium and water handling

Upon a standard salt diet, the plasma potassium level was significantly increased in *Tsc22d3-2*-deficient mice, even though plasma sodium, urinary electrolytes and aldosterone levels are unaltered (**Table S3**). Plasma and urinary osmolarity was also conserved upon standard and sodium-deprived diets, and following water-deprivation (**Table S3**). After feeding a sodium-deprived diet for 10 consecutive days, knockout mice exhibited the same water and food intake with no change in body weight (**Fig. S3**). However, these mice showed significantly increased plasma sodium and decreased potassium levels (**Table S3**; $P< 0.05$), although plasma aldosterone levels were unaffected. In summary, *Tsc22d3-2* knockout mice were generally able to adapt to deprivation of sodium or water even though they developed a subtle deficiency in renal sodium and water handling.

***Tsc22d3-2*-deficiency causes male sterility**

Heterozygous females did not show any obvious fertility problems (see above). In contrast, breeding of knockout males (hemizygous, *Tsc22d3-2*$^{D/y}$, 3-6 months old) to wildtype females (C57BL/6N) never revealed any offspring. We observed the presence of vaginal plugs in spontaneously cycling or hormone-stimulated females (ko male: three plugged out of four versus two plugged out of 4 wt females (wildtype male) indicating that the mating behaviour of the male knockouts was not affected). Since the *Tsc22d3-2* gene is X-linked, we could not obtain homozygous mutant females. Gross histopathological examination of all organs revealed differences only in testis (**Fig. S4**). In adult mice, the testicular mass and size was strikingly reduced (age-matched wt, 0.123± 0.011g

versus ko littermates, 0.023±0.002g, n=7 each group, mean age 19.3 weeks ± 1.7, $P< 0.001$; **Fig. 5*A***;). Until the age of 10 days, testicular histology was nearly indistinguishable between the knockout and control groups. From day 20 onwards, spermatogenesis is progressively affected and in 2 - 6 month-old knockouts, no germ cells or mature spermatozoa could be identified (**Fig. 5*B* and *C***). Plasma level of corticosterone was significantly decreased, while FSH and testosterone were significantly increased and LH was unchanged (**Fig. 5*D***). In 20-day-old knockout mice, the total cell number per seminiferous tubule decreased by about 60% mainly due to the increased number of TUNEL-positive cells while the portion of proliferating cells, as measured by Ki67 staining remained constant (**Fig. 5*E***; $P < 0.001$). At 2 months of age, the number of Sertoli cells per tubule is increased, although at 6 months of age, no difference is no longer evident (**Fig. 5*F***). We found an increased number of interstitial Leydig cells as shown by GATA4 immunostaining and quantification (**Fig. 5*C*** and ***G***). The mRNA transcript levels of somatic (FSHR and GATA4) markers were about 28- and 5-fold increased respectively, while the germ cell marker (MVH) mRNA transcript expression was nearly abolished (**Fig. 5*H***). This finding was not confirmed in other pparγ and pparγ2 expressing organs (**Fig. S5 *C***). Expression of genes in testis, like e.g., *Pparγ, Nr3c1* (GR), and *Klf5* were significantly downregulated, while levels of *Tsc22d1*, *Nr3c4* (AR) and *Klf15* were significantly upregulated **(Fig. 5*I*).** The observed transcriptional downregulation of the direct TSC22D3-2 target gene *Pparγ2,* was accompanied by a reduced protein expression level (**Fig. S5 *A***). Altogether, we have identified a novel and crucial role for TSC22D3-2 in testis development and fertility.

Discussion

Tsc22d3-2 is an X-linked gene, which is constitutively expressed in a variety of mouse, rat and human tissues. The encoded protein, the glucocorticoid-induced leucine zipper (GILZ) was suggested to play roles in the immune system, in adipogenesis and sodium homeostasis. Although TSC22D3-2 was reported to interact with signaling molecules like NF-kB, c-Fos, Raf-1, Ras, ERK1/2, C/EBP, histone deactylase 1 (HDAC1) (see for review Ayroldi and Riccardi, 2009 (1)), little was known about its regulation and *in vivo* physiological roles. In this study, we analyzed a knockout model of TSC22D3-2 with respect to the immune system and immune responses, growth and metabolism, and

for the capacity to regulate ENaC-mediated sodium reabsorption in the kidney following salt-and water-deprived challenges/constraints. The observed data only partially support the suggested role for TSC22D3-2/GILZ in metabolism or sodium handling, while they revealed no important role in the immune system. In contrast, we have shown a crucial novel role for TSC22D3-2/GILZ in male fertility.

Mild phenotype in metabolism, adipogenesis and sodium handling in knockout mice

Glucocorticoids are thought to be implicated in the differentiation of mesenchymal progenitor cells, and factors that block adipogenesis favour osteogenic lineage commitment (13). Despite less body fat in older mice, *Tsc22d3-2*-deficient mice generally do not present severe metabolic alterations, or obvious bone abnormalities (**Fig. S3, Table S1 and S3**). The presence of an increased number of glucagon-positive Langerhans cells in the pancreas may be a compensatory mechanism for the higher plasma insulin levels. This suggests an altered insulin sensitivity (**Fig. 1, Table S2**), although knockout mice react in the normal range to glucose and insulin tolerance tests, and to fasted and refed conditions (**Fig. 1**). Furthermore, adipocyte differentiation is not severely modified in the *Tsc22d3-2*-knockout mice (**Fig. 1**). This is surprising as TSC22D3-2 was reported to bind to the tandem repeat of CCAAT/enhancer-binding protein (C/EBP) binding sites in the *Pparγ2* promoter thereby blocking *Pparγ2* transcription and consequently inducing Pparγ2 adipogenesis ((12)). Indeed, in differentiated knockout adipocytes, we find significantly increased *Pparγ2* and *FabP4* mRNA transcript expression (**Fig. 1*H*)**. Our findings are also in contrast to studies where ectopic expression of TSC22D3-2 inhibited glucocorticoid-induced adipocyte differentiation in 3T3-L1 pre-adipocyte cells (12, 14). Even more surprisingly, in liver and testis from *Tsc22d3-2* knockout mice, the purported increase in *Pparγ2* promoter activation as a consequence of *Tsc22d3-2*-deficiency was not confirmed and, instead, *Pparγ2* mRNA transcript and protein expression levels are downregulated in the testis (**Fig. S5 *A*).** This downregulation in the testis could be biased by a complete loss of germ cells in relation to somatic cells. Alternatively, these observations suggest that additional tissue-specific factors may modulate the transcriptional and translational levels of *Pparγ2*. Indeed, following a high fat diet for 18 weeks, TSC22D3-2 knockout mice were not only protected from weight gain, but also developed

less hepatic steatosis (**Fig. 1*L***). This is in contrast to *in vitro* data that predict an increase in hepatic steatosis in the absence of TSC22D3-2 and an induction of ENaC-mediated transport in a cortical collecting duct cell line (mpkCCDc14; (11)). Even upon various challenges like salt- and water-deprivation, we were unable to observe significant changes compared to the control group, suggesting that TSC22D3-2 does not play an important role in water or ENaC-mediated sodium handling, and in the control of blood pressure and blood volume which is in contrast to previous publications (17, 18). In this context, it has been shown that fluid retention is independent of collecting duct ENaC activity when induced by thiazolidinedione, an agonist of Pparγ (15). In contrast, Pparγ agonists induce sodium and water retention in type II diabetes-treated patients (see for review (16)). Although we cannot exclude compensatory mechanisms, we did not find an upregulation of Tsc22d1 mRNA transcript expression levels; the αENaC mRNA transcript expression level was unchanged (**Fig. S5 *C***). We suggest that ENaC-regulation by GILZ does not play a crucial role in kidney homeostasis.

Immune system and immune responses are not dependent on TSC22D3-2

Glucocorticoids are potent modulators of the immune system, and are therefore used as anti-inflammatory and immunosuppressive drugs. They induce apoptosis of $CD4^+CD8^+$ double positive (DP) cells, which requires gene transcription and coordinated activation of caspases (17, 18). TSC22D3-2 is strongly up-regulated by glucocorticoids in the thymus (2) and might have a dual role in inducing apoptosis of thymocytes and rescuing them from T-cell receptor (TCR)-induced cell death (see for review Ashwell et al, 2000 (19)). Surprisingly, despite the predicted *Tsc22d3-2*-dependent negative regulation of T-cell function, we found no severe impairment of thymus and spleen development (**Fig. 2**). In addition, our data do not support an anti-proliferative activity of TSC22D3-2 on T-lymphocytes, as found in concanavalin A-activated T-lymphocytes (6), nor a negative regulation of erythroid progenitor differentiation (20) but instead a significant increase in erythroblast number (**Fig. 2**).

Following stimulation of peritoneal and BMDMs from TSC22D3-2 knockout mice, secretion of TNF, RANTES, MIP-2 and interleukin-6 was unaltered (**Fig. 3*A-D***). This is in contrast to transgenic

mice that overexpress GILZ in all thymocyte subsets and mature peripheral $CD4^+$ and $CD8^+$ T cells (21). *Tsc22d3-2* mRNA transcript expression levels were up-regulated in spleen and peritoneal macrophages of mice that received restraint stress (22). In the treatment of severe sepsis and septic shock, low-dose glucocorticoids exhibit anti-inflammatory effects as seen by a decrease in the inflammatory response and an increase in anti-inflammatory cytokines (23, 24). Unexpectedly, BMDMs from *Tsc22d3-2*-deficient mice did not secrete less proinflammatory cytokines upon treatment with LPS or Pam3, or after E. coli infection, and were not more resistant to dose-dependent dexamethasone treatment (**Fig. 4**). Our findings thus suggest that glucocorticoid action is not mediated or dependent on TSC22D3-2 in this in vitro sepsis model.

TSC22D3-2 plays a crucial and novel role in testis development and fertility

The most striking and obvious phenotype in TSC22D3-2 knockout mice was the male sterility manifest by the significantly reduced testis size and weight, the absence of germ cells and the increased apoptosis in adult seminiferous tubules (**Fig. 5*E***). Normal spermatogenesis requires both pituitary gonadotrophins, namely luteinizing hormone LH and the follicle stimulating hormone FSH, and the testicular androgen testosterone (see for review Steinberger et al, 1991 (25)). With normal LH and elevated FSH levels (**Fig. 5*D***), we did not observe the anticipated downregulation of FSH and LH secretion (25), suggesting that lack of TSC22D3-2 impairs feedback inhibition of gonadotropin secretion by the pituitary.

Our phenotype strikingly resembles that of *Six5*- and *c-kit*-deficient mice (26, 27). Sarkar and colleagues proposed that *Six5,* via reduced *c-kit* levels contributed to the male reproductive defects in myotonic dystrophy 1 (DM1), although we did not find changes in *six5* mRNA transcript expression level (**Fig. S5 *B***). This is a multisystem disorder characterized by endocrine defects that include testicular and tubular atrophy, oligospermia, Leydig cell hyperproliferation and increased FSH levels, although LH and testosterone levels were unchanged (28). Interestingly, in addition to the significantly lower plasma corticosterone levels, high testosterone levels in the TSC22D3-2 knockout mice may further impair corticosterone activity by downregulation of glucocorticoid receptor expression (**Fig. 5**; (29, 30)). At the same time, the complete loss of germ cell-specific MVH

299 expression and the significant increase in FSHR and GATA4 as somatic markers might well explain
300 the deregulation of genes such as *KLF15* or *Tsc22d1* in the testis (**Fig. 5*H* and *I***). It has been
301 proposed that testosterone exerts its regulating function on spermatogenesis by modifying cortisol-
302 dependent apoptosis (32), coinciding with the significantly higher cell-apoptosis in the knockout
303 mice (**Fig. 5**). In this context, it is interesting to note that androgen receptor knockout mice show a
304 severe disruption of spermatogenesis with the failure of germ cells to progress beyond the early
305 stages of meiosis (33). Although the underlying mechanism is not yet fully understood, Leydig cell
306 hyperproliferation is proposed to present a compensatory mechanism to increase testicular
307 steroidogenesis induced by testosterone insufficiency (34). Since we do not find a higher
308 proliferation rate of the Leydig cell population in the Gilz knockouts, our Leydig cell hyperplasia per
309 intertubular space is only "apparent" and seems not to be altered per tubule. LH seems to be most
310 effective in increasing the number of interstitial cells (35), but FSH might exert a proliferative effect
311 on precursor mesenchymal cells that form Leydig cells postnatally (36-38). In summary, TSC22D3-2
312 is essential for male gametogenesis and exerts a crucial role in the interplay between endocrine
313 stimulation, somatic cell activity and spermatogenesis. The use of germ cell- and sertoli-cell specific
314 conditional knockouts will further help to dissect this crucial role of TSC22D3-2 in germ *via* somatic
315 cells. In addition, use of conditional knockouts might also allow to generate mice lacking TSC22D3-
316 2 in females and thus to directly address effects of this protein in female fertility and physiology.
317
318 In summary, mice lacking TSC22D3-2 are viable and exhibit a significant decrease in plasma
319 cortisol. Our data did not confirm a crucial involvement of TSC22D3-2 in immunity, inflammatory
320 responses or adipogenesis. Functional redundancy by other members of the same family might
321 compensate for this loss, as suggested by the increased *Tsc22d1* mRNA transcript expression in the
322 testis. All other glucocorticoid-dependent organs and tissues analyzed in this study exhibit only
323 minor defects, if any, or a default that might only become visible under challenge conditions.
324 TSC22D3-2-deficient mice might therefore be useful to dissect these glucocorticoid-dependent and –
325 independent processes in the future.
326

Material and Methods

Animals

All animals were housed in a controlled environment with a 14 h light/10 h dark cycle with free access to water and a standard laboratory diet. Males were aged from 3 to 6 months, and were backcrossed to C57BL/6N mice (N4-N6). The control group consisted of age-matched *Tsc22d3-2*$^{+/y}$ and *Tsc22d3-2*$^{lox/y}$ littermates. Mouse experiments were conducted under the approval of local authorities and followed Swiss guidelines.

Generation of conditional and null mutant *Tsc22d3-2* mice

The *Tsc22d3-2* gene (NM_010286.3) was cloned from a 129/Sv mouse genomic BAC library (Incite Genomics, Inc., USA). The following fragments were then subcloned into a modified lox-targeting vector containing 2 loxP and 2 frt sites. First, a 10kb (5' region, containing exon 3) and a 5kb *Eco*RI fragment (3' region, containing exons 4 to 6), were subcloned into pBSII KS(-) and extracted using *Pac*I and *Stu*I restriction enzyme recognition sites. The neomycin resistance gene cassette was flanked by *frt* sites and followed by one *loxP* site (pAT-FRT-K13; (39)) and cloned into an *Eco*RV site (3' of the polyA region). The second *loxP* sequence was introduced in a *Sma*I restriction site created by PCR-based mutagenesis, along with a new diagnostic *Eco*RV restriction site 5' of the third exon. Finally, the thymidine kinase cassette (HSV-tk) was inserted 3' of the homologous region. Further details of cloning are available on request. The targeting vector was linearized with *Pac*I, and transfected into A2 embryonic stem cells (ES cells) of the 129Sv/EV background (40, 41) as described previously (42). G418 and ganciclovir-resistant colonies were expanded and screened by PCR using the following primers; 5' recombination: sense 5'-ATAGCCTGTGCTCTGGAACT-3', antisense, 5'-TTATGGCGCGGGGATATCTA-3' and 3' recombination: sense 5'-GCCTCCGAGGTTGCAGTGTTT-3', antisense 5'-TCGCCTTCTTGACGAGTTCTTC-3'. Targeted clones were confirmed by Southern blot analysis using two external probes (3' probe: a 315 bp fragment isolated from the 3' *Eco*RI clone was isolated by *Stu*I and *Bgl*II and used as a probe on *Eco*RI-digested genomic DNA, and 5' probe: a 1085 bp fragment isolated from the 5' *Eco*RI clone by *Dra*I was used on *Eco*RV-digested genomic DNA). PCR-amplified neomycin sequences were

used as an internal probe. Correctly targeted clones were injected into C57BL/6N blastocyts as described (43). Breeding of *Tsc22d3-2*^{loxneo} mice with Flp mice (44) allowed the excision of the neomycin cassette and with nestin-CRE mice (45) mice to generate mice harbouring the Δ allele. To obtain knockout males (*Tsc22d3-2*$^{\Delta/y}$), heterozygous mutant *Tsc22d3-2*$^{\Delta/+}$ females were crossed with wild type males. *Tsc22d3-2*$^{\Delta/+}$ and *Tsc22d3-2*$^{+/+}$ females, as well as *Tsc22d3-2*$^{+/y}$ and *Tsc22d3-2*$^{\Delta/y}$ males were genotyped by PCR (sense (s1): 5'-CAGGTCTGAGTAACTTGTCC-3', antisense (as): 5'-CAGTCTGTGGTGACCGTTTC-3', sense (s2): 5'-TGACAGCTGCGTTTCTCAGTG-3'); s1, s2 and as were used for genotyping of lox and wt alleles, and s1 and as for the Δ allele. For homologous recombination of the *Tsc22d3-2* gene, the targeting vector was electroporated into ES cells, and 5 independent correctly targeted clones were obtained. **Suppl.Fig. 1B** shows representative Southern blot analyses from targeted ES cell clones digested with *Eco*RV (5' probe) and *Eco*RI (3' probe) that revealed diagnostic fragments of 7.8kb and 2kb, respectively. Three recombined ES cell clones were injected into blastocysts of C57BL6/N mice. Chimeric mice that transmitted the floxed allele to their offspring (*Tsc22d3-2loxneo/+*; **Suppl.Fig. 1C**) were further crossed with the Flp-deleter mice to obtain mice harbouring a floxed (*Tsc22d3-2lox/+*) allele (**Suppl.Fig. 1D**). Following breeding *Tsc22d3-2loxneo/+* mice with the germline deleter strain Nestin-Cre (45), we obtained a *Tsc22d3-2* allele lacking exons 3-6 (*Tsc22d3-2-2Δ/y*; **Suppl.Fig. 1D**). **Suppl.Fig. 1E** illustrates *Tsd22d3-2* expression from the *Tsc22d3-2lox* allele whereas the *Tsc22d3-2Δ* allele did not show any expression.

Breeding strategy

Since the *Tsc22d3-2* gene is X-linked, we did not obtain homozygous mutant females. For all further experiments, in order to obtain male *Tsc22d3-2* knockout animals, we crossed heterozygous mutant females to wildtype males to get age-matched knockout and littermate controls.

Histology and immunohistochemistry

Mice were dissected and organs fixed with buffered 10% formalin (pH 7.2) for 12 hours. Tissues were embedded in paraffin (Leica Microsystems, Wetzlar, Germany) and 2-3 mm sections stained with haematoxylin and eosin (H&E). Testis cellular proliferation was assessed by Ki-67 antibody

(monoclonal rat anti-mouse, Dako M7249, Carpinteria, CA, USA; dilution 1:50) with goat anti-rat HRP secondary antibody (Biosource ALI 3404, Camarillo, CA, USA). Apoptosis was analysed using terminal transferase and Biotin-16-dUTP (TUNEL Enzyme, Roche 11 767 305 001; dilution 1:250 and Biotin-16-dUTP, dilution 1:250; Roche 11 093 070 910, *Roche* Diagnostics GmbH, Mannheim, Germany). Sertoli and Leydig cells were labelled with the rabbit anti-GATA4 (ab84593; Abcam plc Cambridge, UK; dilution 1:140) with EnVision (DakoCytomation, Glostrup, Denmark) used as secondary antibody (46). Pancreas sections were incubated with antibodies against insulin (Linco 4011-01, Linco Research Inc., St. Charles, MO, USA; dilution 1:6000) and glucagon (Linco 4030-01F, Linco Research Inc., St. Charles, MO, USA; dilution 1:6000), and then revealed with Fuchsin (Kit DAKO K0625, Dako, Denmark; dilution 1:50) and DAB (Kit DAKO K3468, Dako, Denmark; dilution 1:50), respectively. GILZ1 and GILZ2 proteins were labelled with the polyclonal Tsc22d3-2 antibody as described (4).

Quantitative real-time PCR

Tissues were collected and quickly snap frozen in liquid nitrogen and kept at -80 °C until use. Total RNA was extracted from tissues with the RNeasy Mini Kit or Qiazol (Qiagen, Valencia, CA, USA). Total RNA (1 μg) was subjected to reverse transcription using SuperScript II (Invitrogen/Life Technologies Corporation**,** Carlsbad, CA, USA) following the manufacturer's instructions. The resulting cDNA was used as a template for quantitative PCR (qPCR). Results were normalized using the glyceraldehyde 3-phosphate dehydrogenase (GAPDH) or RNA polymerase II. Quantitative real-time analysis of selected genes was performed using the ABI Prism 7500 Fast Real-Time PCR System, SYBR Green as DNA binding dye for the detection of PCR products or the TaqMan probe technology (Applied Biosystems/Life Technologies Corporation**,** Carlsbad, CA, USA). Intron-spanning primers were designed (Microsynth AG, Switzerland) (see **Table S4** for oligonucleotides). The cycling conditions were 95 °C for 10 min, followed by 40 cycles of 95 °C for 15 s, and 60 °C for 1 min. To detect and eliminate possible primer–dimer artifacts, the dissociation curve was generated by adding a cycle of 95 °C for 15 s, 60 °C for 1 min and 95 °C for 15 s. All primer sets produced

amplicons of the expected size and their identity was also verified by migration of the PCR products on agarose gel. Quantification was done by measuring the ΔΔCt normalized to the reference gene. All measurements were done at least in triplicate, n = 3 mice per group, data represent average ± SEM.

Western blot analyses

Tissue samples were collected from dexamethasone (55 μg/100g body weight)-treated and non-treated control and knockout mice. The dexamethasone was administered intraperitoneally 3-4 hours before euthanasia. Tissue lysis was performed in ice-cold urea (8M) using the TissueLyser (Qiagen, Valencia, CA, USA). Protein levels were quantified using the Pierce BCA Protein Assay Reagent (Thermo Fisher Scientific, Waltham, MA, USA) with BSA as a standard. Equal amounts of protein extracts were resolved by 12% SDS-PAGE and electro-transferred onto a Protran nitrocellulose membrane (Whatman/GE Healthcare, Piscataway, NJ, USA). Blots were blocked in tris-buffered saline containing 0.1% Tween (TBS-T) supplemented with 4% milk powder and immunoblotted using anti-Tsc22d3-2 antibody, as described previously (4).. The blots were stripped and reprobed with GAPDH antibody (Chemicon/Millipore, Billerica, MA, USA) as a loading control; n = 2 mice per genotype.

Hormone measurements and metabolic parameters

Plasma aldosterone, corticosterone, and testosterone levels were assayed using commercially available kits as described previously (57, 58, 59). To avoid stress-induced increases in plasma hormone levels, animals were trained in a 1-2 week-period with handling (habituation) before sacrifice. For plasma aldosterone and corticosterone measurements, mice ($n \geq 7$, 3- to 4-month-old) were killed by rapid decapitation between 4-6 pm. Blood was collected in EDTA tubes, immediately centrifuged and stored at -20^{o}C until assayed for hormone level determination. Plasma aldosterone levels were measured according to standard procedure using the Coat-A-Count RIA kit (Siemens Medical Solutions Diagnostics, Ballerup, Denmark). Mice samples exhibiting values greater than

1200 pg/ml were previously diluted using a serum pool with a low aldosterone concentration (<50 pg/ml). Corticosterone levels were measured by RIA (IBL, Hamburg, Germany), the rat FSH IRMA kit (n° AHR004) and the rat LH RIA (n° AHR002) were obtained from IDS (Liege, Belgium). Total testosterone levels in non-extracted serum were assayed using a kit from ICN, Biomedicals, INC., Costa Mesa, CA 92626 (cat. n° 07-189102; 100 tubes; Testo DA Kit, now MP Biomedicals, Eschwege, Germany). The standard curves ranged between 2 and 200 ng/ml for FSH, 0.25 and 15 ng/ml for LH, and 0.1 and 10 ng/ml for testosterone. Intra- and inter-assay coefficients of variation (CVs) of all three assays were less than 5% and 10%, respectively. Body weight (weekly) and body composition on individual 2.5- and 15-month-old mice were analysed as described (see also SI). Plasma glucose, insulin levels were determined and glucose and insulin tolerance test were determined as described (see also SI).

Metabolic parameters; body weight was measured on a weekly basis over the whole study. Body composition was analyzed on individual 2.5- and 15-month-old mice under light gaz anesthesia (1-2 % isoflurane), by quantitative nuclear magnetic resonance using an EchoMRI Whole Body Composition Analyzer (EchoMedical Systems, Houston, TX, USA). Data for individual mice were obtained by averaging results from two consecutive measurements. Plasma glucose levels in the fed, 15h fasted or 6h-refed states were measured with a glucometer (Ascensia Breeze2, Bayer, Switzerland). Plasma insulin levels were determined from tail-tip bleedings by ELISA (Ultrasensitive Mouse insulin ELISA, Mercodia AB, Uppsala, Sweden).

Glucose tolerance test; after a 15-hour overnight fasting period, 6-month-old mice were injected i.p. with 1.5 mg/g glucose. Plasma glucose levels were measured 30 minutes before and punctually during 120 minutes after administration ($n \geq 6$ per group).

Insulin tolerance test; following 4 hours of food removal (9am-1pm), age-matched 7-month-old mice were injected intraperitoneally with 0.8 mU/g insulin. Blood samples were obtained from tail-tip bleedings, and plasma glucose levels were measured with a glucometer (Ascensia Breeze 2, Bayer, Switzerland).

Adipocyte differentiation; Mouse embryonic fibroblasts (MEFs) were generated as described (47) (48, 49) from 13.5-day-old embryos obtained from heterozygous mutant female *Tsc22d3-2*$^{+/\Delta}$ mated

to wild type males. Briefly, after removal of head and visceral organs (used for genotyping), embryos were minced and trypsinized for 30 minutes at 37 °C. Embryonic fibroblasts were then plated and maintained in DMEM (with 10% fetal calf serum (FCS) (Life Technologies), 100 U/ml penicillin and 100 µg/ml streptomycin) at 37°C in an atmosphere of 5% CO_2. All experiments were performed with *Tsc22d3-2* wild-type and knockout MEFs after 15-20 passages. For adipocyte differentiation, 2-day-postconfluent cells (day 0) were transferred to DMEM supplemented with 10% FCS, 0.5 mM 3-isobutyl-1-methylxanthine, 1 µM dexamethasone and 1 µg/ml insulin (all from Sigma) and 1µM rosiglitazone (Alexis Biochemicals) for 2 days. Medium was renewed every 2 days with DMEM containing 10% FCS, 1 µg/ml insulin and 1 µM rosiglitazone. To visualize lipid accumulation, cells were stained at day 8 (D8) with Oil Red O (50). Briefly, cells were washed with phosphate-buffered saline (PBS), fixed with 3.7% formaldehyde solution for 1 hour and stained with Oil Red O for 1 hour using a 60:40 (v/v) dilution in water of a 0.5% stock solution (in isopropanol). Cells were then washed twice with PBS and twice with water. MEFs were pooled from $n = 2$ per genotype. Experiments were performed in triplicate.

Flow cytometry and monoclonal antibodies

Thymocyte, lymph node and spleen single cell suspensions were prepared by standard methods and stained for FACS analysis as described (see also SI). Briefly, thymocyte, lymph node and spleen single cell suspensions were preincubated in 50% anti-mouse FcR (CD16/32; clone 2.4.G.2) culture supernatant and then stained with the following monoclonal antibody conjugates: CD4 (RM-4.5 or GK1.5)-FITC, -PE-Cy5 or PE-Cy7; CD8a (53.6.7)-FITC or Alexa 647; CD11b (M1/70)-FITC, PE-Cy5 or Alexa 647; CD24 (M1/69)-PE; CD25 (PC61.5)-Alexa 700 or APC-Alexa 750; CD41 (MWReg30)-FITC or -PE; CD44 (IM781)-PE-Cy7 or Pacific Blue; CD45R/B220 (RA3-6B2)-FITC, PE-Texas Red or PE-Cy7; CD62L (Mel14)-FITC; CD71 (R17217)-PE; CD122 (5H4)-PE; CD117 (2B8)-APC; F4/80 (BM8)-APC Alexa750, Gr1 (RB6-8C5)-FITC, Alexa 647 or Alexa 700; Ter119-FITC or APC-Alexa 750; TCRb (H57)-FITC, PE-Cy5 or APC-Alexa750; TCRgd (GL3)-FITC or PE-Cy5. DN1 ($CD117^+CD44^+CD25^-$), DN2 ($CD117^+CD44^+CD25^+$), DN3 ($CD117^-CD44^-CD25^+$), DN4 ($CD117^-CD44^-CD25^-$), ISP ($CD4^-CD8^+TCRb^-$), gdT cells, DP (double positive, $CD4^+CD8^+$),

CD8 SP (single positive, $CD4^-CD8^+$), CD4 SP ($CD4^-CD8^+$). All FITC conjugates were purified and conjugated in the Ludwig Institute with the exception of CD41-FITC, which was purchased from BD Biosciences (San Jose, CA, USA). All Alexa 647 conjugates were prepared using the Alexa 647 conjugation kit from Invitrogen (Carlsbad, CA, USA). All other monoclonal antibody conjugates were purchased from eBioscience (San Diego, CA, USA). Intracellular staining for TCRb was performed after first surface staining with all monoclonal antibodies. After fixation and permeabilization in Cytofix/Cytoperm (BD Biosciences, San Jose, CA, USA), the cells were incubated overnight at 4°C in 1x Permwash solution (BD Biosciences, San Jose, CA, USA) containing TCRb-PE-Cy5 and then washed in 1x Permwash and resuspended in PBS/3% FCS for FACS analysis. Samples were analyzed on either a FACS Canto™ or a FACS LSR II™ (both Becton Dickinson, San Jose, CA, USA) and the data analyzed with FlowJo™ software (TreeStar, Ashland, OR, USA).

Inflammation experiments

Three-month-old mice were sacrificed (n = 3, each group) and bone marrow-derived dendritic cells (BMDC), bone marrow-derived macrophages (BMDM) and thioglycolate-elicited peritoneal macrophages (TEPM) were prepared and stimulated as previously described (51-55). Briefly, LPS, MSU, ATP, Candida and CpG stimuli were obtained from InvivoGen (San Diego, CA, USA), ELISA kits from R&D Systems (Minneapolis, MN, USA). Bone marrow-derived macrophages (BMDMs) were obtained as previously described (13, 14) and cultured in IMDM containing 10% FCS (Sigma-Aldrich), 100 UI/ml penicillin, 100 µg/ml streptomycin and 50 µM 2-mercaptoethanol. Cells were preincubated for 1 h with dexamethasone (Sigma-Aldrich) prior to stimulation with 10 ng/ml of *Salmonella minnesota* Ultra Pure lipopolysaccharide (LPS) (List Biologicals Laboratories), 10 µg/ml Pam_3CSK_4 lipopeptide (EMC microcollections), 5x 10^7 heat-inactivated *Escherichia coli* (*E. coli*) J5 or 0.1 mM CpG oligodeoxynucleotide (CpG ODN, Coley Pharmaceutical Group). Cell culture supernatants were collected to measure the concentration of IL-12p40 by ELISA (BD Biosciences), and the concentration of TNF and IL-6 by bioassay (56). Splenocytes (5 x 10^5 cells in 200 µl) were seeded in 96-well plates coated with 1µg/ml anti-CD3 and anti-CD28 antibodies (BD Biosciences) or

stimulated with 2.5µg/ml concanavalin A (Con A, Sigma-Aldrich) in the presence or absence of dexamethasone. IL-2 levels in cell culture supernatants collected after 24 h were measured by ELISA assay (BD Biosciences).

Sodium-restriction diet and water deprivation

Mice (20–24 weeks old) were fed with a standard salt diet (0.17% sodium, Ssniff Spezialdiäten GmbH, Soest, Germany) followed by 12 days with a sodium-deficient diet (<0.01% sodium, Ssniff Spezialdiäten GmbH, Soest, Germany*)*. The 23 hours water deprivation was performed under normal-salt diet. Body weight, food and water intake were measured during the experiment. Spot urine and serum/blood samples were collected before and after each experiment, and osmolarity as well as sodium, potassium and creatinine composition were analyzed at the Laboratoire Central de Chimie Clinique of the University Hospital (CHUV, Lausanne, Switzerland).

Statistical analysis

Data were analyzed using the Student's *t* test for comparison between the groups. Results are expressed as the mean ± SEM. A P value < 0.05 was considered as statistically significant.

Acknowledgements

We thank Jürg Tschopp (who passed away during the preparation of this manuscript) for his active contribution to this study, and whose contribution was financed by Swiss National Science Foundation (grant 3100A0-128658/1), Association "Institute for Arthritis Research" and Louis-Jeantet Prize for Medicine to JT. This work has been furthermore supported by the Fondation Emma Muschamps, the Swiss National Science Foundation to EH and TR (FNS 310030_132744), and the Leducq Foundation to EH and BR. VP is recipient of a Marie Curie fellowship. We thank the Transgenic Animal Facility, the Mouse Metabolic Evaluation Facility, the Mouse Pathology Platform, the Cellular Imaging Facility and the Flow Cytometry Facility (all at the University of Lausanne) for their help and services.

549 **Addendum**

550 After submission of our manuscript, a knockout of the long-glucocorticoid-induced leucine zipper
551 (L-GILZ) was published (60) that exhibits a similar, but not identical testis phenotype compared to
552 our complete knockout.

553

554

555 **REFERENCES**

556

557 1. Ayroldi E, Riccardi C 2009 Glucocorticoid-induced leucine zipper (GILZ): a new important
558 mediator of glucocorticoid action. FASEB J 23:3649-3658

559 2. D'Adamio F, Zollo O, Moraca R, Ayroldi E, Bruscoli S, Bartoli A, Cannarile L, Migliorati
560 G, Riccardi C 1997 A new dexamethasone-induced gene of the leucine zipper family protects
561 T lymphocytes from TCR/CD3-activated cell death. Immunity 7:803-812

562 3. Mittelstadt PR, Ashwell JD 2001 Inhibition of AP-1 by the glucocorticoid-inducible protein
563 GILZ. J Biol Chem 276:29603-29610

564 4. Soundararajan R, Wang J, Melters D, Pearce D 2007 Differential activities of glucocorticoid-
565 induced leucine zipper protein isoforms. J Biol Chem 282:36303-36313

566 5. Ayroldi E, Migliorati G, Bruscoli S, Marchetti C, Zollo O, Cannarile L, D'Adamio F,
567 Riccardi C 2001 Modulation of T-cell activation by the glucocorticoid-induced leucine
568 zipper factor via inhibition of nuclear factor kappaB. Blood 98:743-753

569 6. Ayroldi E, Zollo O, Bastianelli A, Marchetti C, Agostini M, Di Virgilio R, Riccardi C 2007
570 GILZ mediates the antiproliferative activity of glucocorticoids by negative regulation of Ras
571 signaling. J Clin Invest 117:1605-1615

572 7. Delfino DV, Agostini M, Spinicelli S, Vito P, Riccardi C 2004 Decrease of Bcl-xL and
573 augmentation of thymocyte apoptosis in GILZ overexpressing transgenic mice. Blood
574 104:4134-4141

575 8. Cohen N, Mouly E, Hamdi H, Maillot MC, Pallardy M, Godot V, Capel F, Balian A, Naveau
576 S, Galanaud P, Lemoine FM, Emilie D 2006 GILZ expression in human dendritic cells
577 redirects their maturation and prevents antigen-specific T lymphocyte response. Blood
578 107:2037-2044

579 9. Hamdi H, Bigorgne A, Naveau S, Balian A, Bouchet-Delbos L, Cassard-Doulcier AM,
580 Maillot MC, Durand-Gasselin I, Prevot S, Delaveaucoupet J, Emilie D, Perlemuter G 2007
581 Glucocorticoid-induced leucine zipper: A key protein in the sensitization of monocytes to
582 lipopolysaccharide in alcoholic hepatitis. Hepatology 46:1986-1992

10. Muller OG, Parnova RG, Centeno G, Rossier BC, Firsov D, Horisberger JD 2003 Mineralocorticoid effects in the kidney: correlation between alphaENaC, GILZ, and Sgk-1 mRNA expression and urinary excretion of Na+ and K+. J Am Soc Nephrol 14:1107-1115

11. Soundararajan R, Zhang TT, Wang J, Vandewalle A, Pearce D 2005 A novel role for glucocorticoid-induced leucine zipper protein in epithelial sodium channel-mediated sodium transport. J Biol Chem 280:39970-39981

12. Shi X, Shi W, Li Q, Song B, Wan M, Bai S, Cao X 2003 A glucocorticoid-induced leucine-zipper protein, GILZ, inhibits adipogenesis of mesenchymal cells. EMBO Rep 4:374-380

13. Beresford JN, Bennett JH, Devlin C, Leboy PS, Owen ME 1992 Evidence for an inverse relationship between the differentiation of adipocytic and osteogenic cells in rat marrow stromal cell cultures. J Cell Sci 102 (Pt 2):341-351

14. Batchvarova N, Wang XZ, Ron D 1995 Inhibition of adipogenesis by the stress-induced protein CHOP (Gadd153). EMBO J 14:4654-4661

15. Vallon V, Hummler E, Rieg T, Pochynyuk O, Bugaj V, Schroth J, Dechenes G, Rossier B, Cunard R, Stockand J 2009 Thiazolidinedione-induced fluid retention is independent of collecting duct alphaENaC activity. J Am Soc Nephrol 20:721-729

16. Blazer-Yost BL 2010 PPARgamma Agonists: Blood Pressure and Edema. PPAR Res 2010:785369

17. Cifone MG, Migliorati G, Parroni R, Marchetti C, Millimaggi D, Santoni A, Riccardi C 1999 Dexamethasone-induced thymocyte apoptosis: apoptotic signal involves the sequential activation of phosphoinositide-specific phospholipase C, acidic sphingomyelinase, and caspases. Blood 93:2282-2296

18. Marchetti MC, Di Marco B, Cifone G, Migliorati G, Riccardi C 2003 Dexamethasone-induced apoptosis of thymocytes: role of glucocorticoid receptor-associated Src kinase and caspase-8 activation. Blood 101:585-593

19. Ashwell JD, Lu FW, Vacchio MS 2000 Glucocorticoids in T cell development and function*. Annu Rev Immunol 18:309-345

20. Kolbus A, Blazquez-Domingo M, Carotta S, Bakker W, Luedemann S, von Lindern M, Steinlein P, Beug H 2003 Cooperative signaling between cytokine receptors and the glucocorticoid receptor in the expansion of erythroid progenitors: molecular analysis by expression profiling. Blood 102:3136-3146

21. Cannarile L, Fallarino F, Agostini M, Cuzzocrea S, Mazzon E, Vacca C, Genovese T, Migliorati G, Ayroldi E, Riccardi C 2006 Increased GILZ expression in transgenic mice up-regulates Th-2 lymphokines. Blood 107:1039-1047

22. Wang Y, Lu Y, Yu D, Chen F, Yang H, Zheng SJ 2008 Enhanced resistance of restraint-stressed mice to sepsis. J Immunol 181:3441-3448

23. Briegel J, Kellermann W, Forst H, Haller M, Bittl M, Hoffmann GE, Buchler M, Uhl W, Peter K 1994 Low-dose hydrocortisone infusion attenuates the systemic inflammatory response syndrome. The Phospholipase A2 Study Group. Clin Investig 72:782-787

24. Prigent H, Maxime V, Annane D 2004 Science review: mechanisms of impaired adrenal function in sepsis and molecular actions of glucocorticoids. Crit Care 8:243-252

25. Steinberger A 1991 Effects of temperature on the biochemistry of the testis. Adv Exp Med Biol 286:33-47

26. Rothschild G, Sottas CM, Kissel H, Agosti V, Manova K, Hardy MP, Besmer P 2003 A role for kit receptor signaling in Leydig cell steroidogenesis. Biol Reprod 69:925-932

27. Sarkar PS, Paul S, Han J, Reddy S 2004 Six5 is required for spermatogenic cell survival and spermiogenesis. Hum Mol Genet 13:1421-1431

28. Vazquez JA, Pinies JA, Martul P, De los Rios A, Gatzambide S, Busturia MA 1990 Hypothalamic-pituitary-testicular function in 70 patients with myotonic dystrophy. J Endocrinol Invest 13:375-379

29. Chen S, Wang J, Yu G, Liu W, Pearce D 1997 Androgen and glucocorticoid receptor heterodimer formation. A possible mechanism for mutual inhibition of transcriptional activity. J Biol Chem 272:14087-14092

30. Kerr JE, Beck SG, Handa RJ 1996 Androgens modulate glucocorticoid receptor mRNA, but not mineralocorticoid receptor mRNA levels, in the rat hippocampus. J Neuroendocrinol 8:439-447

31. Kimura N, Mizokami A, Oonuma T, Sasano H, Nagura H 1993 Immunocytochemical localization of androgen receptor with polyclonal antibody in paraffin-embedded human tissues. J Histochem Cytochem 41:671-678

32. Russell LD, Clermont Y 1977 Degeneration of germ cells in normal, hypophysectomized and hormone treated hypophysectomized rats. Anat Rec 187:347-366

33. De Gendt K, Swinnen JV, Saunders PT, Schoonjans L, Dewerchin M, Devos A, Tan K, Atanassova N, Claessens F, Lecureuil C, Heyns W, Carmeliet P, Guillou F, Sharpe RM, Verhoeven G 2004 A Sertoli cell-selective knockout of the androgen receptor causes spermatogenic arrest in meiosis. Proc Natl Acad Sci U S A 101:1327-1332

34. Mylchreest E, Sar M, Wallace DG, Foster PM 2002 Fetal testosterone insufficiency and abnormal proliferation of Leydig cells and gonocytes in rats exposed to di(n-butyl) phthalate. Reprod Toxicol 16:19-28

35. Dombrowicz D, Sente B, Reiter E, Closset J, Hennen G 1996 Pituitary control of proliferation and differentiation of Leydig cells and their putative precursors in immature hypophysectomized rat testis. J Androl 17:639-650

36. Benton L, Shan LX, Hardy MP 1995 Differentiation of adult Leydig cells. J Steroid Biochem Mol Biol 53:61-68

37. Hardy MP, Zirkin BR, Ewing LL 1989 Kinetic studies on the development of the adult population of Leydig cells in testes of the pubertal rat. Endocrinology 124:762-770

38. Saez JM 1994 Leydig cells: endocrine, paracrine, and autocrine regulation. Endocr Rev 15:574-626

39. Trumpp A, Refaeli Y, Oskarsson T, Gasser S, Murphy M, Martin GR, Bishop JM 2001 c-Myc regulates mammalian body size by controlling cell number but not cell size. Nature 414:768-773

663 40. Hummler E, Merillat AM, Rubera I, Rossier BC, Beermann F 2002 Conditional gene
664 targeting of the Scnn1a (alphaENaC) gene locus. Genesis 32:169-172
665 41. Reis LF, Ruffner H, Stark G, Aguet M, Weissmann C 1994 Mice devoid of interferon
666 regulatory factor 1 (IRF-1) show normal expression of type I interferon genes. EMBO J
667 13:4798-4806
668 42. Hummler E, Barker P, Gatzy J, Beermann F, Verdumo C, Schmidt A, Boucher R, Rossier
669 BC 1996 Early death due to defective neonatal lung liquid clearance in alpha-ENaC-deficient
670 mice. Nat Genet 12:325-328
671 43. Porret A, Merillat AM, Guichard S, Beermann F, Hummler E 2006 Tissue-specific
672 transgenic and knockout mice. Methods Mol Biol 337:185-205
673 44. Rodriguez CI, Buchholz F, Galloway J, Sequerra R, Kasper J, Ayala R, Stewart AF,
674 Dymecki SM 2000 High-efficiency deleter mice show that FLPe is an alternative to Cre-
675 loxP. Nat Genet 25:139-140
676 45. Buchholz F, Refaeli Y, Trumpp A, Bishop JM 2000 Inducible chromosomal translocation of
677 AML1 and ETO genes through Cre/loxP-mediated recombination in the mouse. EMBO Rep
678 1:133-139
679 46. Jelinic P, Stehle JC, Shaw P 2006 The testis-specific factor CTCFL cooperates with the
680 protein methyltransferase PRMT7 in H19 imprinting control region methylation. PLoS Biol
681 4:e355
682 47. Hansen JB, Petersen RK, Larsen BM, Bartkova J, Alsner J, Kristiansen K 1999 Activation of
683 peroxisome proliferator-activated receptor gamma bypasses the function of the
684 retinoblastoma protein in adipocyte differentiation. J Biol Chem 274:2386-2393
685 48. Yang YC, Hsu HK, Hwang JH, Hong SJ 2003 Enhancement of glucose uptake in 3T3-L1
686 adipocytes by Toona sinensis leaf extract. Kaohsiung J Med Sci 19:327-333
687 49. Lukas J, Bartkova J, Rohde M, Strauss M, Bartek J 1995 Cyclin D1 is dispensable for G1
688 control in retinoblastoma gene-deficient cells independently of Cdk4 activity. Mol Cell Biol
689 15:2600-2611

690 50. Ramirez-Zacarias JL, Castro-Munozledo F, Kuri-Harcuch W 1992 Quantitation of adipose
691 conversion and triglycerides by staining intracytoplasmic lipids with Oil red O.
692 Histochemistry 97:493-497
693 51. Gross O, Gewies A, Finger K, Schafer M, Sparwasser T, Peschel C, Forster I, Ruland J 2006
694 Card9 controls a non-TLR signalling pathway for innate anti-fungal immunity. Nature
695 442:651-656
696 52. Gross O, Poeck H, Bscheider M, Dostert C, Hannesschlager N, Endres S, Hartmann G,
697 Tardivel A, Schweighoffer E, Tybulewicz V, Mocsai A, Tschopp J, Ruland J 2009 Syk
698 kinase signalling couples to the Nlrp3 inflammasome for anti-fungal host defence. Nature
699 459:433-436
700 53. Muruve DA, Petrilli V, Zaiss AK, White LR, Clark SA, Ross PJ, Parks RJ, Tschopp J 2008
701 The inflammasome recognizes cytosolic microbial and host DNA and triggers an innate
702 immune response. Nature 452:103-107
703 54. Roger T, Lugrin J, Le Roy D, Goy G, Mombelli M, Koessler T, Ding XC, Chanson AL,
704 Reymond MK, Miconnet I, Schrenzel J, Francois P, Calandra T 2011 Histone deacetylase
705 inhibitors impair innate immune responses to Toll-like receptor agonists and to infection.
706 Blood 117:1205-1217
707 55. Roger T, Froidevaux C, Le Roy D, Reymond MK, Chanson AL, Mauri D, Burns K, Riederer
708 BM, Akira S, Calandra T 2009 Protection from lethal gram-negative bacterial sepsis by
709 targeting Toll-like receptor 4. Proc Natl Acad Sci U S A 106:2348-2352
710 56. Roger T, David J, Glauser MP, Calandra T 2001 MIF regulates innate immune responses
711 through modulation of Toll-like receptor 4. Nature 414:920-924
712 57. Christensen BM, Perrier R, Wang Q, Zuber AM, Maillard M, Mordasini D, Malsure S,
713 Ronzaud C, Stehle JC, Rossier BC, Hummler E 2010 Sodium and potassium balance depends
714 on alpha ENaC expression in connecting tubule. J Am Soc Nephrol 21 :1942-1951
715 58. Cederroth CR, Zimmermann C, Beny JL, Schaad O, Combepine C, Descombes P, Doerge
716 DR, Pralong FP, Vassalli JD, Nef S 2010 Potential detrimental effects of a phytoestrogen-
717 rich diet on male fertility in mice. Mol Cell Endocrinol 321 :152-160

718 59. Romero Y, Meikar O, Papaioannou MD, Conne B, Grey C, Weier M, Pralong F, De Massy
719 B, Kaessmann H, Vassalli JD, Kotaja N, Nef S 2011 Dicer 1 depletion in male germ cells
720 leads to infertility due to cumulative meiotic and spermiogenic defects PLoS One 6 :e25241.
721 60. Bruscoli S, Velardi E, Di Sante M, Bereshchenko O, Venanzi A, Coppo M, Berno V, Memeli
722 M G, Colella R, Cavaliere A, Riccardi C 2011, Long-Glucocorticoid-induced leucine Zipper
723 (L-GILZ) interacts with Ras pathway and contributes to spermatogenesis control. J Biol
724 Chem; doi:10.1074/jbc.M111.316372
725

Figure legends

Figure 1. *Tsc22d3-2*$^{\Delta/y}$ mice show reduction in weight, mild hyperinsulinemia and resistance to high fat diet. (***A***) Body weight values of control (black) and knockout mice (white circles; $n \geq 8$ per group; *$P < 0.05$). (***B***), glucose (1.5 mg/g BW) and (***C***) insulin (0.8 mU/g) tolerance tests; $n \geq 6$ per group). (***D***), Glucagon (brown, a cells) and insulin (rose, b cells) expression in pancreatic islets of Langerhans from control (left) and knockout (right) mice; ($n = 3$ mice per group; bar = 50 mm). (***E***), Ratio of glucagon-positive Langerhans cells per islet (left) and plasma glucagon levels (right panel; ($n \geq 15$ images, $n = 3$ mice per group) in control (black) and knockout mice (white columns; **$P < 0.001$). (***F***) Body weight values of control (black) and knockout mice following 18 weeks of high fat diet (white circles; $n \geq 11$ per group). (***G***) Plasma insulin concentration in control and knockout mice upon normal (chow; black: control; white: knockout) and high fat (control: grey; knockout: red columns) diet in fed, fasted and refed conditions; $n \geq 10$ per group. (***H***) Representative pictures of H&E stained liver sections from control (ctrl, left) and knockout (ko, right panel) mice upon chow (upper) and high fat diet (lower panel) following 18 consecutive weeks ($n = 3$ mice per group; bar size indicated). (***I, J***) Two days after confluence, MEF cells were induced (D, differentiated) or not (ND, not differentiated) to differentiate into adipocytes. (***I***), overview and (***J***), higher magnification of oil-red o-stained cells at 8 days post-induction. (***K***) and (***L***), Quantitative RT-PCR of *Tsc22d3-2*, *Pparγ2*, *Pparγ* and *FabP4* from non-differentiated (ND) and differentiated (D) MEF cells from control (ctrl) and knockout (ko) mice (***K***) and *Pparγ2*, *Pparγ, Tsc22d1*, adiponectin, aP2 (= *FabP4*), KLF15 in fat tissues isolated from control (black) and knockout (white columns, n = 3 animals; ***L***). Experiments were performed in triplicate; *$P < 0.05$, ***$P < 0.001$.

Figure 2. *Tsc22d3-2*$^{\Delta/y}$ mice exhibit minor deficiencies in thymus, spleen and lymph nodes. (***A***), Thymus size in 10-, 20-day-old and 56-146 days old mice (n ≥ 7). (***B***), Absolute cell numbers (x10^6) for indicated thymocyte subsets in 10, 20 and 56-146 days old mice. (***C***), Absolute cell numbers (x10^6) for indicated splenocyte subsets. (***D***), Absolute cell numbers (x10^6) for indicated lymph node subsets. Black bars: control; white bars: knockout mice, data represent average ± SEM; n≥ 3 mice per group, 10-week-old males. *$P < 0.05$ when compared to control.

754

755 **Figure 3.** *Tsc22d3-2*$^{\Delta/y}$ mice show no impairment of inflammatory responses. Peritoneal and bone
756 marrow-derived cytokine secretion. (***A and B***), ELISA for TNF (***A and C***), and MIP-2 (***B and D***)
757 following ± stimulation of peritoneal macrophages with LPS supplemented by indicated stimuli. (***C***
758 ***and D***) Stimulation of bone marrow-derived macrophages (see ***A*** and ***B***) ± dexamethasone (0.2 mM).
759 Data are shown as mean values of duplicated stimulations ± SEM from 3 mice per group. (***E-G***)
760 Quantification of IL-1b (***E***), TNF (***F***) and Rantes (***G***) production in bone marrow-derived cells
761 primed with 10 ng/ml of LPS ± Dex for indicated periods prior to inflammasome activation by 100
762 ng/ml of MSU for 5h or 5 mM of ATP for 1h ; (***E***)), heat-inactivated Candida cells (***F***) or 1µM CpG
763 for 6h (***G***). Data are shown as mean values of triplet stimulations ± SEM and representative for three
764 independent experiments with a total of 6 control and 6 knockout mice.
765

766 **Figure 4.** *Tsc22d3-2*-deficient bone marrow-derived macrophages (BMDMs) are not susceptible to
767 the immunosuppressive effects of dexamethasone. Control and knockout (***A-C***) and splenocytes (***D-***
768 ***E***) are incubated with or without (med) increasing concentrations of dexamethasone (DEX, 10^{-10}-10^{-7}
769 M) and indicated stimuli (***A-C***) IL-2 concentrations collected 4 h (TNF) or 18 h (IL-6, IL-12p40, IL-
770 2) after stimulation. Cytokine concentrations in cells stimulated without dexamethasone are set at 1
771 for normalization. Data are means ± SD of triplicates samples from one experiment comprising two
772 mice per experimental condition and are representative of two experiments.
773

774 **Figure 5.** *Tsc22d3-2* knockout males are sterile. (***A***), Representative pictures from 2 and 6 month old
775 control (above) and knockout (below) adult testes. ***(B),*** **H&E-stained paraffin sections and** ***(C)***,
776 immunohistochemistry of Sertoli and Leydig cells counterstained with H&E-stained paraffin sections
777 from control (ctrl) and knockout (ko) testes. (***B*** **and** ***C***), Note absence of mature spermatozoa (white
778 arrow head) and hyperproliferation of Leydig cells (black arrow) in the knockouts. (***C***), Higher
779 resolution image (rabbit anti-GATA4 antibody) and counterstaining with hematoxylin (blue nuclei);
780 elongated spermatids (white arrowhead) in controls. (***D***), Corticosterone (cort), follicle-stimulating
781 (FSH), luteinizing hormone (LH) and testosterone (testo) hormone levels in plasma ($n \geq 10$ animals

per group, 3-4 months old). (***E***), Total number of cells per seminiferous tubule (n ≥ 20 tubules per group; left). Ratio of Ki-67 positive cells divided by total cell number, middle) and ratio of TUNEL positive cells divided by total cell number per seminiferous tubule, n = 18 tubules, right). (***F***), quantification of Sertoli cells per tubule (***F;*** n ≥ 25 tubules) and Leydig cells in the inter-tubular space (***G;*** n ≥ 27) at 2 (N = 2) and 6 months (N = 4 animals). (***H***), qRT-PCR of *FSHR, GATA4 and MVH* control (black) and knockout animals (white columns). (***I***), qRT-PCR of *Pparγ2, Tsc22d1,* GR, AR, KLF5, KLF15 in testis from control (black) and knockout animals (white columns). (Scale bar: (***A***), 1 mm; (***B***), 100 µm and (***C***) 50 µm); **P* < 0.05, ***P* < 0.01 and ****P* < 0.001.

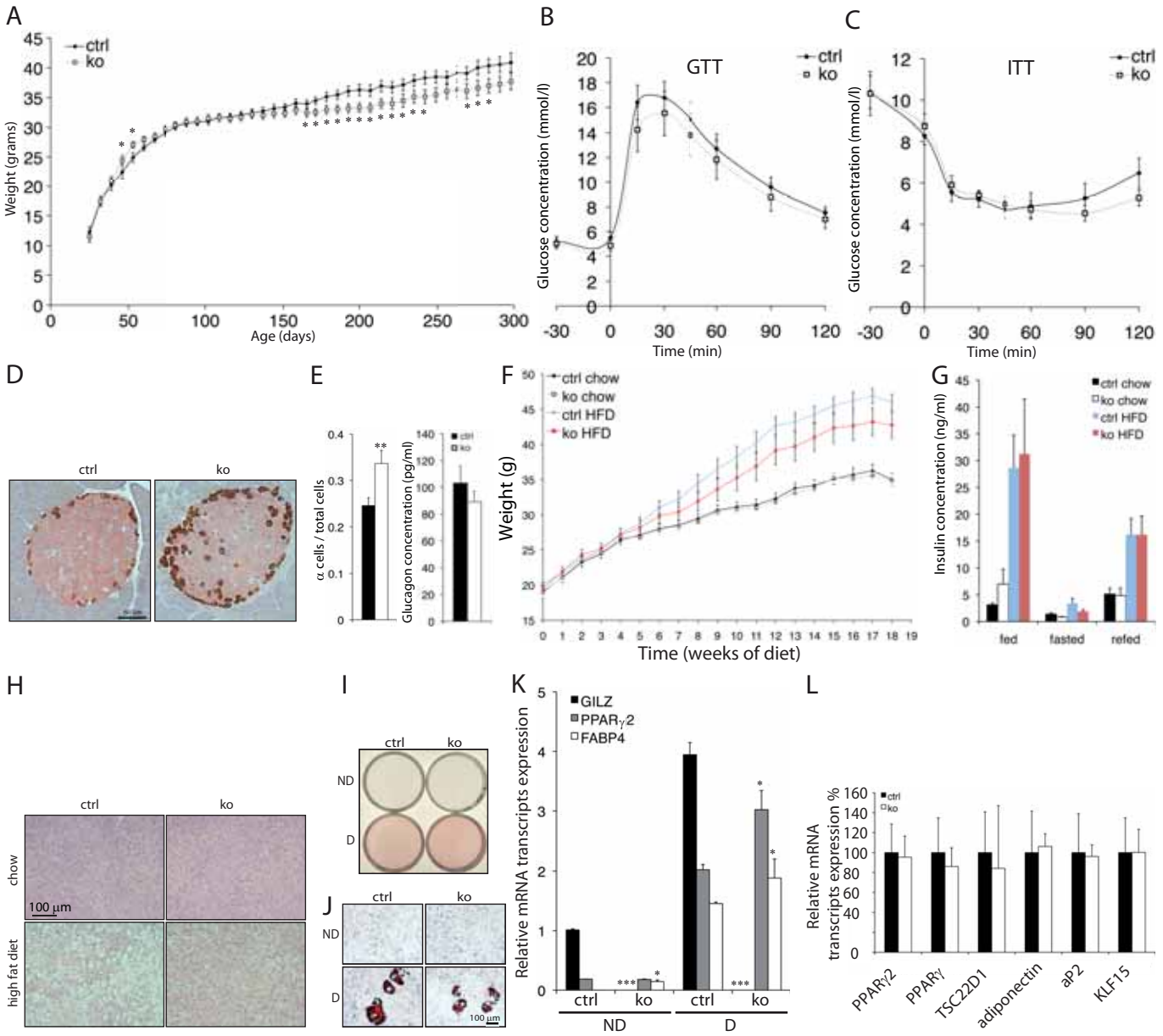
A
ctrl
ko
Weight (grams)
Age (days)
B
GTT
Glucose concentration (mmol/l)
Time (min)
C
ITT
Glucose concentration (mmol/l)
Time (min)
D
ctrl
ko
E
α cells / total cells
Glucagon concentration (pg/ml)
F
ctrl chow
ko chow
ctrl HFD
ko HFD
Weight (g)
Time (weeks of diet)
G
Insulin concentration (ng/ml)
fed
fasted
refed
H
chow
high fat diet
100 µm
I
ND
D
J
K
GILZ
PPARγ2
FABP4
Relative mRNA transcripts expression
L
Relative mRNA transcripts expression %
PPARγ2
PPARγ
TSC22D1
adiponectin
aP2
KLF15

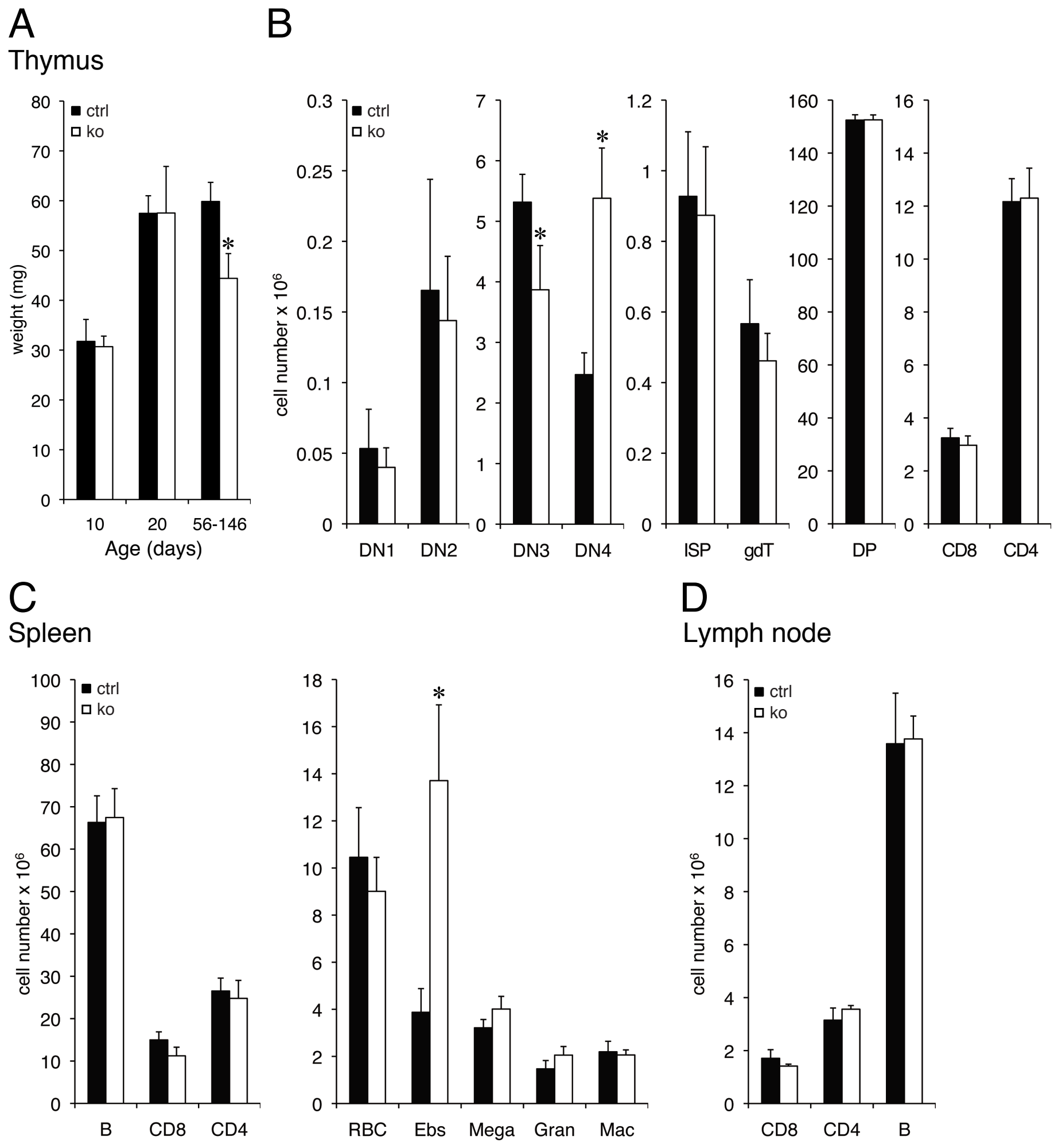
A
Thymus
ctrl
ko
weight (mg)
Age (days)
10
20
56-146
B
cell number x 10^6
DN1
DN2
DN3
DN4
ISP
gdT
DP
CD8
CD4
C
Spleen
B
CD8
CD4
RBC
Ebs
Mega
Gran
Mac
D
Lymph node
CD8
CD4
B

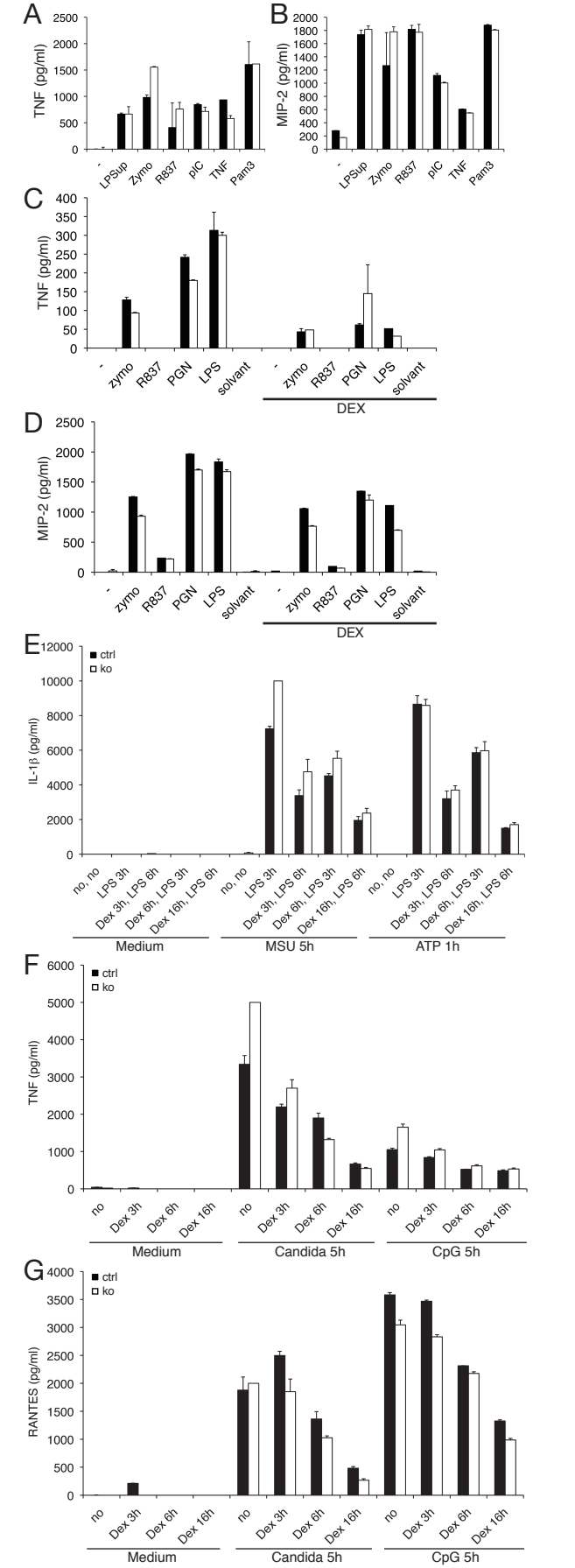
A
TNF (pg/ml)
2500
2000
1500
1000
500
0
-
LPSup
Zymo
R837
pIC
TNF
Pam3
B
MIP-2 (pg/ml)
2000
1800
1600
1400
1200
1000
800
600
400
200
0
-
LPSup
Zymo
R837
pIC
TNF
Pam3
C
TNF (pg/ml)
400
350
300
250
200
150
100
50
0
-
zymo
R837
PGN
LPS
solvant
-
zymo
R837
PGN
LPS
solvant
DEX
D
MIP-2 (pg/ml)
2500
2000
1500
1000
500
0
-
zymo
R837
PGN
LPS
solvant
-
zymo
R837
PGN
LPS
solvant
DEX
E
IL-1β (pg/ml)
12000
10000
8000
6000
4000
2000
0
ctrl
ko
no, no
LPS 3h
Dex 3h, LPS 6h
Dex 6h, LPS 3h
Dex 16h, LPS 6h
Medium
MSU 5h
ATP 1h
F
TNF (pg/ml)
6000
5000
4000
3000
2000
1000
0
ctrl
ko
no
Dex 3h
Dex 6h
Dex 16h
Medium
Candida 5h
CpG 5h
G
RANTES (pg/ml)
4000
3500
3000
2500
2000
1500
1000
500
0
ctrl
ko
no
Dex 3h
Dex 6h
Dex 16h
Medium
Candida 5h
CpG 5h

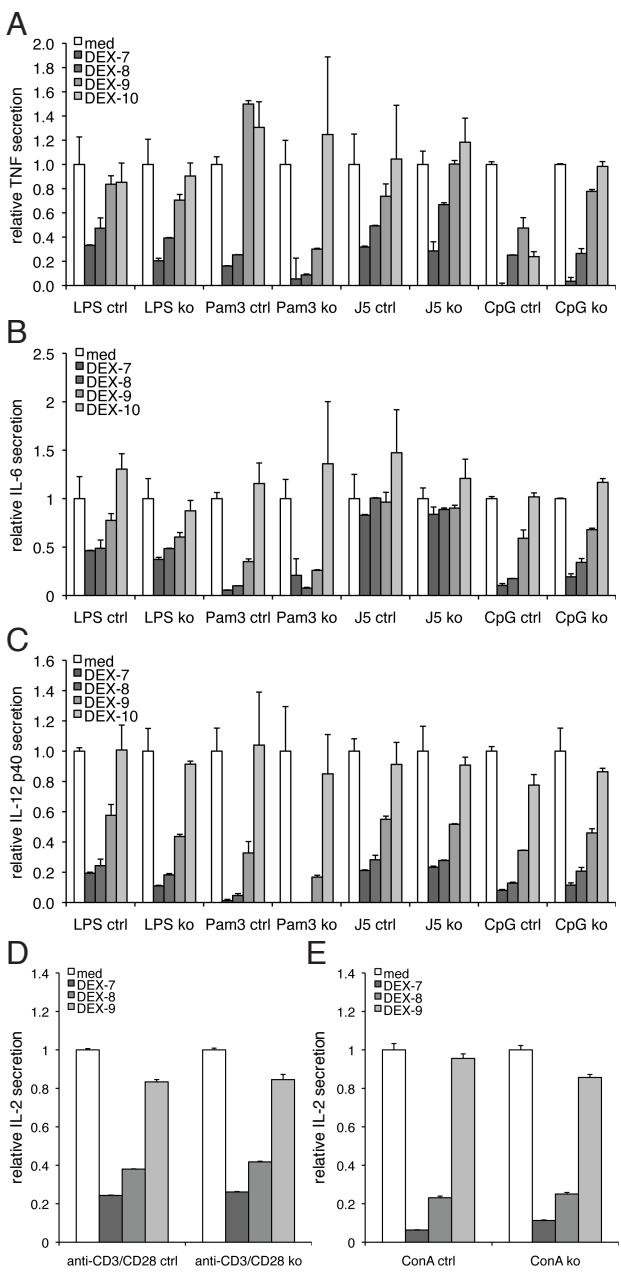
A
med
DEX-7
DEX-8
DEX-9
DEX-10
relative TNF secretion
2.0
1.8
1.6
1.4
1.2
1.0
0.8
0.6
0.4
0.2
0.0
LPS ctrl
LPS ko
Pam3 ctrl
Pam3 ko
J5 ctrl
J5 ko
CpG ctrl
CpG ko
B
med
DEX-7
DEX-8
DEX-9
DEX-10
relative IL-6 secretion
2.5
2
1.5
1
0.5
0
LPS ctrl
LPS ko
Pam3 ctrl
Pam3 ko
J5 ctrl
J5 ko
CpG ctrl
CpG ko
C
med
DEX-7
DEX-8
DEX-9
DEX-10
relative IL-12 p40 secretion
1.6
1.4
1.2
1
0.8
0.6
0.4
0.2
0.0
LPS ctrl
LPS ko
Pam3 ctrl
Pam3 ko
J5 ctrl
J5 ko
CpG ctrl
CpG ko
D
med
DEX-7
DEX-8
DEX-9
relative IL-2 secretion
1.4
1.2
1
0.8
0.6
0.4
0.2
0
anti-CD3/CD28 ctrl
anti-CD3/CD28 ko
E
med
DEX-7
DEX-8
DEX-9
relative IL-2 secretion
1.4
1.2
1
0.8
0.6
0.4
0.2
0
ConA ctrl
ConA ko

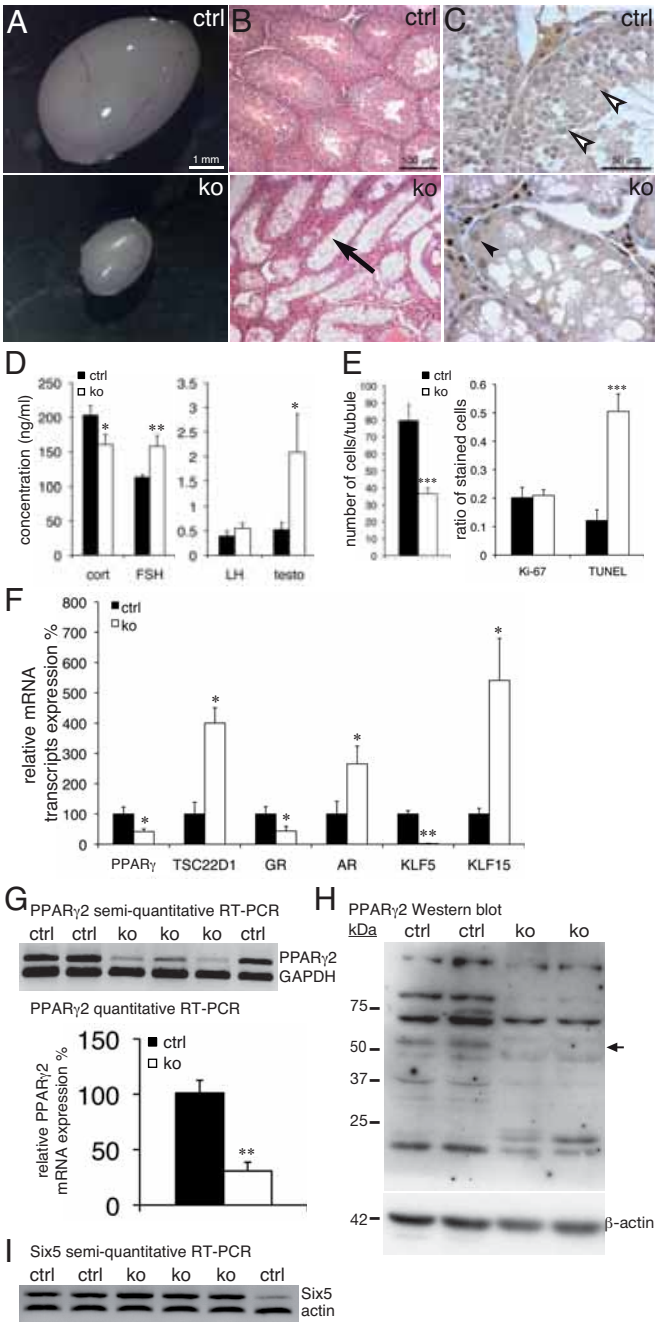
A
ctrl
1 mm
B
ctrl
C
ctrl
ko
ko
ko
D
ctrl
ko
concentration (ng/ml)
cort
FSH
LH
testo
E
number of cells/tubule
ratio of stained cells
Ki-67
TUNEL
F
relative mRNA transcripts expression %
PPARγ
TSC22D1
GR
AR
KLF5
KLF15
G
PPARγ2 semi-quantitative RT-PCR
ctrl ctrl ko ko ko ctrl
PPARγ2
GAPDH
PPARγ2 quantitative RT-PCR
relative PPARγ2 mRNA expression %
H
PPARγ2 Western blot
kDa
ctrl ctrl ko ko
75
50
37
25
42
β-actin
I
Six5 semi-quantitative RT-PCR
ctrl ctrl ko ko ko ctrl
Six5
actin